


## RESEARCH ARTICLE

# Structuring of 2-oleodipalmitin at the air interface from all-atom, united-atom, and coarse-grained molecular dynamics simulations

Moritz Kindlein<sup>1</sup> | Ekaterina Elts<sup>1</sup> | Peter Horlacher<sup>2</sup> | Heiko Briesen<sup>1</sup> | Tobias Koch<sup>1</sup> 

<sup>1</sup>School of Life Sciences Weihenstephan, Chair of Process Systems Engineering, Technical University of Munich, Freising, Germany

<sup>2</sup>BASF Personal Care and Nutrition GmbH, Illertissen, Germany

## Correspondence

Tobias Koch, School of Life Sciences Weihenstephan, Chair of Process Systems Engineering, Technical University of Munich, Gregor-Mendel-Str. 4, 85354 Freising, Germany.

Email: t.b.koch@tum.de

## Abstract

This study employs classical molecular dynamics (MD) simulations to investigate the behavior of 1,3-dipalmitoyl-2-oleoyl glycerol (POP), a typical triglyceride found in food at the air interface. The investigation utilizes three force fields (FF) with varying levels of detail, including all-atom, united-atom, and coarse-grained simulations, to elucidate the structural evolution of POP at the air interface. The results confirm that the structuring processes observed in nonfood triglyceride systems also occur in POP. Aliphatic chains orient toward the air phase, while glycerol backbones face the inner triglyceride phase. Additionally, the study observes the formation of clusters of glycerol head groups at the interface, and the choice of the FF significantly affects the simulated morphological structure. The Berger FF exhibits the most substantial structuring effects after 200 ns of simulation, followed by the General AMBER FF, while the Martini FF shows the weakest effects. Number density plots of aliphatic chains and glycerol backbones at different temperatures monitor the evolution of structuring effects over time and determine the approach toward equilibrium conditions. The temperatures investigated include the solid state of POP at ambient temperature (293 K), the liquid state at human body temperature (310 K), and a typical processing temperature of the chocolate conching process (333 K).

*Practical Applications:* Tailored molecular design of interfaces according to their purpose in food.

## KEYWORDS

air interface, food foam, lipids, structuring, molecular dynamics, triglycerides

## 1 | INTRODUCTION

Fat-air interfaces<sup>[1,2]</sup> are present in fat-based food foams, such as whipped cream, ice cream, dessert toppings, and others.<sup>[3]</sup> Dairy

foams, in particular, are complex molecular mixtures and contain carbohydrates, fat particles, emulsifiers, and air bubbles.<sup>[4–8]</sup> Within these systems, fat-air interfaces often occur as the fat particles adsorb at the initial water-air interface to stabilize it. Such a system is shown in Figure 1 (according to Ref. [9]).

**Abbreviations:** POP, 1,3-dipalmitoyl-2-oleoyl glycerol; FF, force field; GAFF, general AMBER force field; MD, molecular dynamics; TG, triglycerides.

This is an open access article under the terms of the Creative Commons Attribution-NonCommercial-NoDerivs License, which permits use and distribution in any medium, provided the original work is properly cited, the use is non-commercial and no modifications or adaptations are made.

© 2023 The Authors. European Journal of Lipid Science and Technology published by Wiley-VCH GmbH

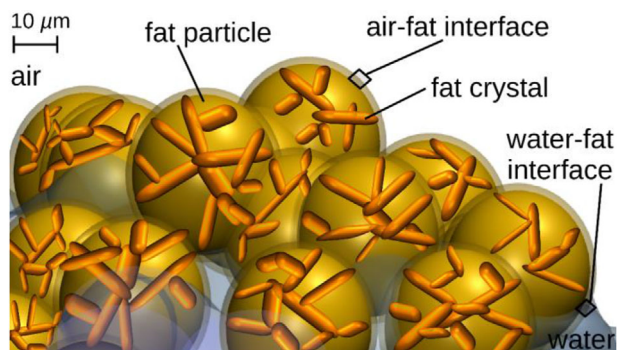


**FIGURE 1** Schematic representation of fat particle coalescence and adsorption at the air-water interface. Fat particles (yellow) containing crystallites forming cohesive clusters (orange) within extended flog structures as found in products with high, solid fat content like ice cream or whipped cream. Notably, POP triglycerides invert orientation at fat-air interfaces compared to water-fat interfaces (corona zones).

The fat particles shown are known to contain crystalline solid fat, depending on the specific system. In their initially aqueous environment, it seems plausible that a phospholipid membrane monolayer surrounds the fat particles to build a stable interface with water. When fat particles come into contact with air, it is less clear what happens with the amphiphilic membrane phospholipids. Since air is also a hydrophobic phase, it seems unlikely that the membrane remains the same at that interface as it is present at the interface with water.

Phospholipids can form stable bilayers or lipid vesicles due to their amphiphilic nature, which arises from a hydrophilic head and a hydrophobic tail, facilitating maximized hydrophilic interactions. In contrast, triglycerides, characterized by a less hydrophilic glycerol backbone, tend to arrange themselves into lamellae structures with extended domains in crystallites or micellar structures containing disordered amorphous regions.<sup>[1,2]</sup> Nevertheless, under certain conditions, triglycerides can undergo structuring processes leading to the partial formation of layered structures. For instance, these structuring effects occur at the bare fat-air interface, where both phases are hydrophobic.

The resulting liquid fat-air interface is highlighted in Figure 1, which gives a schematic representation of a typical food foam interface and visualizes the limited extension of the simulation box. The current study provides insights into the molecular structure on the fat side of this interface with the help of molecular dynamics simulations, where Newton's equations of motion are solved to calculate the dynamic evolution of the systems.

The liquid fat phase studied here is a pure 1,3-dipalmitoyl-2-oleoyl glycerol (POP) phase, a commonly occurring food triglyceride (see Figure 2). Triglycerides consist of a glycerol backbone connected to three aliphatic chains via ester bonds. The aliphatic chains can either contain covalent double bonds (in which case they are unsaturated) or only covalent single bonds (in which case they are saturated). POP has two saturated and one unsaturated aliphatic chain. The glycerol

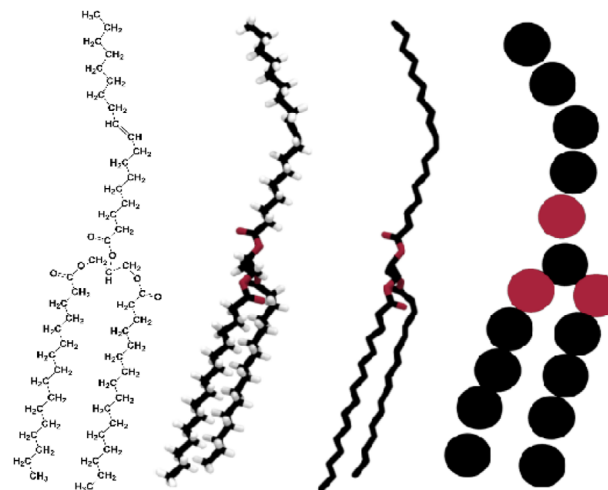


**FIGURE 2** Representation of POP with the different levels of detail: chemical structure, all-atom, united-atom, and coarse-grained models.

backbone, which connects the aliphatic chains, is more polar than the aliphatic chains and, thus, is also the most polar part of the whole triglyceride molecule.<sup>[10,11]</sup> These physicochemical characteristics make a particular orientation at specific interfaces likely.

To capture the physical behavior on different time scales, molecular dynamics simulations can be performed with varying degrees of resolution using molecular modeling approaches at all-atom, united-atom, and coarse-grained levels. In each case, different parameter sets and energy terms, called force fields (FF), are applied to describe interatomic and intermolecular interactions. The force fields provide contributions for bonded and nonbonded interactions to the potential energy for all interaction centers in the system.

Starting from the chemical structure, in an all-atom representation of a classical force field, each atom is considered a mass point with an associated partial charge (Figure 2). United-atom (UA) force fields reduce the number of degrees of freedom in the system by including hydrogen atoms in the heavy atoms to which they have a covalent bond. Coarse-grained force fields map various heavy atoms to one coarse-grained bead (e.g., four-to-one).

The used united-atom and coarse-grained FFs were derived by fitting the parameters of the interaction potentials to a broad base of experimental properties. The reduced number of degrees of freedom, due to the lower number of interaction centers within the molecules, give the united-atom and coarse-grained force fields the substantial advantage of less computational cost while omitting chemical details. All three presented modeling approaches allow the derivation of macroscopic thermodynamic properties based on the microscopic behavior of atomic-scale building blocks according to the laws of statistical thermodynamics.<sup>[12,13]</sup>

Two molecular dynamics simulation studies can be found in the literature, where the molecular structures of triglycerides at the air interface were investigated concerning other systems. Wizert et al.<sup>[1]</sup> investigated the organization of lipids in the human eye tear film by employing the coarse-grained Martini FF.<sup>[14,15]</sup> They found that oleic

triglycerides are predominantly present at the surface of the tear film. By plotting the number density along the box axis perpendicular to the fat-air interface, they found that triglycerides are oriented with aliphatic chains toward the air interface. Tascini et al.<sup>[2]</sup> used the united-atom Berger FF to investigate human sebum palmitoleic acid triglycerides.<sup>[16]</sup> They discovered that the Berger model satisfactorily represents the surface tension of triglycerides at the air interface, indicating the model's suitability for investigating triglyceride-air interfaces. The triglycerides directly in contact with air were shown to orient their aliphatic chains toward the air. In addition to the coarse-grained Martini FF and united-atom Berger FF mentioned above, this study also employs the all-atom General AMBER FF (GAFF, Figure 2). Molecular dynamics studies show the applicability of GAFF to food systems,<sup>[17-20]</sup> and it is applied here to evaluate it in this context further.

Several molecular dynamics studies can be found in literature where similar systems as those presented here are studied in a food manufacturing context. A few examples are presented to highlight the suitability of the simulation method. Emulsifier-induced interfacial ordering of triglycerides present at the fat-water interface has been investigated with the Martini FF. The resulting structures were shown to act as nucleation templates for triglycerides.<sup>[21]</sup> Detailed molecular modeling studies on food-relevant triglyceride systems were carried out by the Milano group. A coarse-grained model for triglycerides was developed,<sup>[22]</sup> and a multiscale approach to studying the liquid-solid transition of triglycerides was presented.<sup>[23]</sup> In cooperation with the Marangoni group, detailed insights into mixed triglyceride crystallization<sup>[24]</sup> and eutectic behavior were given.<sup>[25]</sup>

The remainder of this paper is organized as follows: Section 2 describes the setups of the molecular dynamics simulations, including simulation parameters for the different FFs, system building, and a description of the equilibration procedure. Additionally, the simulation analysis methods are explained. Section 3 presents the study's results, and Section 4 offers a critical discussion. In Section 5, a conclusion of the study is given.

## 2 | MATERIALS AND METHODS

### 2.1 | Molecular dynamics simulations and force fields

The GROMACS software version 5.1.1<sup>[26]</sup> is used for all molecular dynamics simulations of the presented work. The leap-frog algorithm<sup>[27]</sup> is used to integrate Newton's equations of motion. For all-atom simulations, the GAFF<sup>[28]</sup> molecular parameters are calculated with the ACPYPE<sup>[29]</sup> and Antechamber<sup>[30,31]</sup> tools. AM1-BCC charges<sup>[32]</sup> are computed with the semiempirical quantum chemistry method (SQM),<sup>[33]</sup> which delivers semiempirical Mulliken charges by AM1 calculation<sup>[34,35]</sup> followed by a bond charge correction (BCC).<sup>[36]</sup> A time step of 2 fs is used, and cut-offs for all short-range interactions are set to 0.9 nm. The particle-mesh-Ewald method (PME)<sup>[37]</sup> is used for long-range electrostatic interactions. For united-atom simulations,

the Berger parameters<sup>[16]</sup> are used and accessed via the homepage of Peter Tieleman.<sup>[38]</sup> Based on the FF parameters for phospholipids given there, the molecular model of the triglyceride POP is derived by exchanging the phospholipids' head group with a third aliphatic chain. Again, a time step of 2 fs is used, and the PME method<sup>[37]</sup> is applied for long-range electrostatic interactions.

A short-range interaction cut-off radius of 1.2 nm is employed. For coarse-grained simulations, the Martini FF is used.<sup>[14,15]</sup> Molecular parameters available for download from the Martini homepage<sup>[39]</sup> are used, along with a time step of 10 fs. Long-range electrostatic interactions are calculated with the reaction field potential, as suggested by the FF developers.<sup>[15]</sup> A short-range interaction cut-off of 1.1 nm is applied for electrostatic and van der Waals interactions.

512 POP molecules were inserted randomly into the simulation box for each system. The following equilibration procedure was performed to ensure the fat-air interface systems were at the desired temperature and pressure. Initially, an energy minimization with the steepest descent algorithm was performed to eliminate high potential interactions due to steric hindrances. Subsequently, NVT equilibration was performed for 2 ns to allow for a first aggregation of the POP molecules and reach the desired temperatures. In the case of the Berger FF, the Bussi et al. velocity-rescale thermostat<sup>[40]</sup> is used. The Berendsen thermostat<sup>[41]</sup> is applied for GAFF and Martini FF simulations, as it is known to relax very quickly even though it samples a pseudo canonical ensemble.

A subsequent isothermal-isobaric equilibration was performed to reach the desired atmospheric pressure of 1 bar for 10 ns. To control temperature and pressure, the Berendsen thermostat and barostat<sup>[41]</sup> were utilized for Martini and GAFF simulations, and the velocity-rescale thermostat and Parrinello-Rahman barostat<sup>[42]</sup> were used for the Berger simulations. Subsequently, the next equilibration step in the isothermal-isobaric ensemble was performed with the Bussi et al. velocity-rescale thermostat and the Parrinello-Rahman barostat for all the different FF setups for 200 ns. Such a long equilibration time allows us to reasonably sample the pure triglyceride phase and subsequently compare the results with those obtained at the introduced air interface. During this step, the potential energy of the systems was monitored. It should be noted that the equilibrium was achieved only for the Martini FF simulations. For the final production runs, the simulation boxes were elongated in one direction to obtain the desired triglyceride-air interface (where the air is represented as a vacuum according to molecular dynamics simulations from the literature<sup>[1,2]</sup>). The production runs were performed in a canonical ensemble with a duration of 200 ns for GAFF and Berger FF and 5  $\mu$ s for Martini FF, and the structure evolved according to the introduced fat-air interface. This simulation procedure directly implies that the structures are not in equilibrium at the beginning of the production run. The evolution of the molecular structures was tracked in detail and is described in Section 2.2. The GAFF and the Berger FF did not reach equilibrium during the simulation time. Nevertheless, several solid results could be obtained. This is described in Section 3.2 in detail.

All described simulation steps were performed at 293 K, 310 K, and 333 K. 293 K resembles ambient temperature and thus, it is a relevant

temperature for the solid state of POP in a food context. 310 K resembles human body temperature where POP is in its liquid state, which is relevant in a food context. 333 K resembles a typical food processing temperature, for example, the conching process of chocolate, where POP is one of the three main molecular components of cocoa butter.

## 2.2 | Number density calculation and equilibrium analysis of structuring effects

Throughout the paper, the term structuring is used to describe the molecular orientation and alignment of the POP molecules at the air interface. The investigation examines how the molecules orient their glycerol backbones and aliphatic chains in relation to the interface. On the one hand, this structuring is analyzed by visual inspection of the molecular trajectories and, on the other hand, by calculating the number density of aliphatic chains and glycerol backbones of POP along the box  $x$ -axis, which is perpendicular to the fat-air interface. When distinct peaks in the number density plots are visible, the structuring is described as strong, and accordingly weaker when no distinct peaks are observed. When number density plots of different FFs are compared, they are normalized by dividing by the total number of atoms or beads of the specific group in the simulation box. This number varies (despite the same number of molecules) according to the molecular representation of the FF. In the all-atom FF simulations, only the heavy atoms are used for number density calculations since hydrogen atoms are strictly bound to the carbon atoms; therefore, they have no meaningful impact on the number density distributions, where glycerol backbones are compared to the aliphatic chains. For the united-atom FF and the coarse-grained FF, all beads are considered. Number densities are calculated according to the following equation:

$$\langle \rho_n(x) \rangle_{t_i}^{t_{i+1}} = \frac{\langle n(x) \rangle_{t_i}^{t_{i+1}}}{\Delta x \cdot n_g} \quad (1)$$

$\langle \rho_n(x) \rangle_{t_i}^{t_{i+1}}$  is the average number density in a time interval  $\Delta t = 5$  ns between  $t_i$  and  $t_{i+1}$ . Trajectory snapshots are collected at 0.5 ps intervals, resulting in a total of 10 000 frames for the time average  $\langle n(x) \rangle_{t_i}^{t_{i+1}}$ . This time average represents the number of molecules within the time interval  $\Delta t$  in a box slice along the  $x$ -axis, where the width of the slice is denoted as  $\Delta x$ . The box is separated into 500 volume slices along the  $x$ -axis.  $n_g$  is the total number of atoms or beads of the investigated groups in the simulation box. Division by  $n_g$  is conducted to normalize all number density distributions to ensure that the zeroth moment of each distribution is one, no matter how many beads or atoms represent the aliphatic chains and the glycerol backbones.

To get a measure of the equilibrium state of the structuring effects, the development of the number density distribution functions of the glycerol backbones is further analyzed. While the number density is nearly constant along the  $x$ -axis after system building, it develops three distinct peaks during the simulations. These peaks represent the high number of glycerol backbones at certain points along the simulation box  $x$ -axis due to the structuring at the interface. Once the structur-

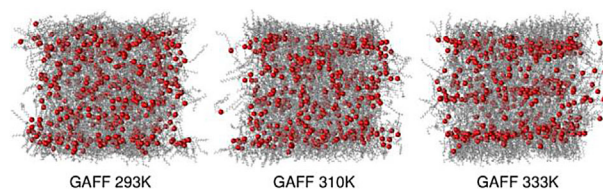


**FIGURE 3** Snapshots after 200 ns simulation time of the GAFF systems at 293 K (left), 310 K (center), and 333 K (right). Oxygen is represented by red spheres, and carbons of the glycerol backbone are represented by gray spheres. Aliphatic chains are shown as gray lines.

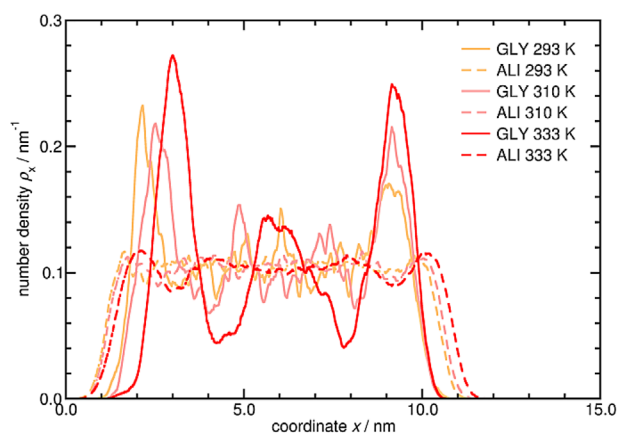


**FIGURE 4** GAFF number density of the glycerol backbones (GLY) and aliphatic chains (ALI) along the  $x$ -axis of the simulation box for the investigated temperatures in the last 5 ns of the simulations.

ing is finished, the height of those peaks remains roughly constant, only prone to thermal fluctuations. The number density functions consist of 500 discrete data points, resulting in high numbers at the local maxima. In order to eliminate these and to detect the three real maxima, the number density functions are smoothed using a moving average filter with a span of 20, as implemented in MATLAB software. Subsequently, the average value of the three highest peaks  $\langle \rho_{n,peaks} \rangle_{t_i}^{t_{i+1}}$  is calculated in Equation (2):

$$\langle \rho_{n,peaks} \rangle_{t_i}^{t_{i+1}} = \frac{\langle \rho_n(x_{max1}) \rangle_{t_i}^{t_{i+1}} + \langle \rho_n(x_{max2}) \rangle_{t_i}^{t_{i+1}} + \langle \rho_n(x_{max3}) \rangle_{t_i}^{t_{i+1}}}{3} \quad (2)$$

## 3 | RESULTS

### 3.1 | Structuring of triglycerides at the air interface

All performed simulations reveal that the aliphatic chains of the triglyceride molecules at the interface orient toward the air phase. Snapshots of all nine simulated systems (after 200 ns simulation time) are shown in Figure 3 for GAFF, Figure 5 for Berger FF, and Figure 7 for Martini FF. In these figures, the air interfaces are on the top and bottom sides of the systems. On the left and right sides, as well as in the direction

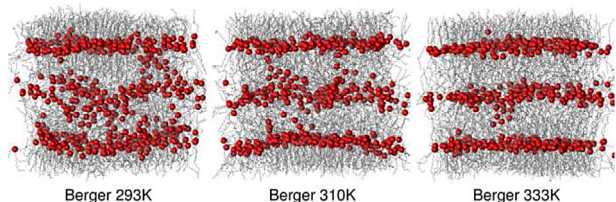


**FIGURE 5** Snapshots after 200 ns simulation time of the Berger FF systems at 293 K (left), 310 K (center), and 333 K (right). Oxygen is represented by red spheres and carbons of the glycerol backbone are represented by black spheres. Aliphatic chains are represented as gray lines.

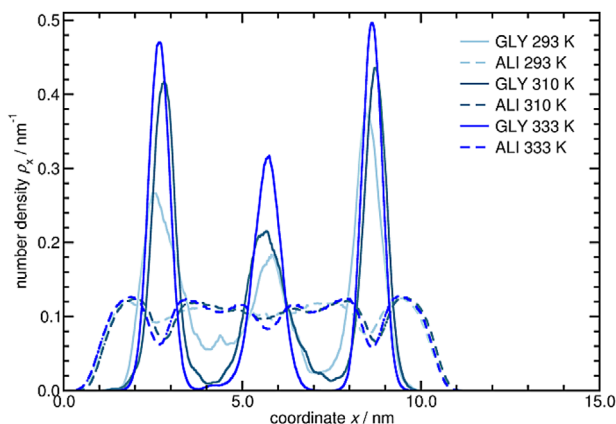


**FIGURE 6** Berger FF number density of the glycerol backbones (GLY) and aliphatic chains (ALI) along the  $x$ -axis of the simulation box for the investigated temperatures in the last 5 ns of the simulations.

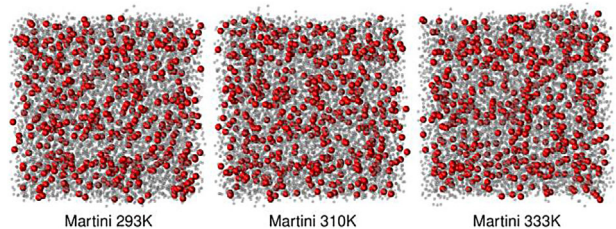


**FIGURE 7** Snapshots after 200 ns simulation time of the Martini FF systems at 293 K (left), 310 K (center), and 333 K (right). Ester beads are shown as red and glycerol beads as gray spheres. Aliphatic chains are shown in transparent sphere representation.

of the drawing sheet, the fat phase continues directly due to periodic boundaries. Figures 4, 6, and 8 show the corresponding number density plots of the glycerol backbones and aliphatic chains of all nine simulated systems in the last 5 ns of the production run simulations, within the same force field series. They provide a quantification of the structuring effects. The standard deviation of the number density from the statistical averaging over 10 intervals of 0.5 ns each is about 2.7% of the nominal value and is not displayed in the figures for clarity. These plots show the normalized number density (according to Equation 1) of the glycerol backbone and aliphatic chain atoms (or beads) along the box axis perpendicular to the interface.

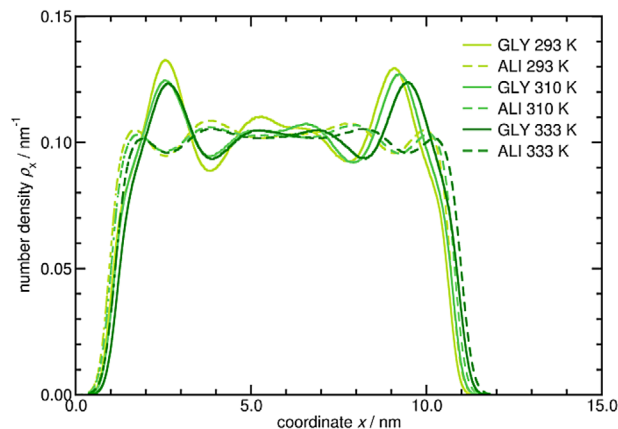


**FIGURE 8** Martini FF number density of the glycerol backbones (GLY) and aliphatic chains (ALI) along the  $x$ -axis of the simulation box for the investigated temperatures in the last 5 ns of the simulations.

Figures 3 and 4 illustrate the results of the simulations at different temperatures with GAFF. At all temperatures, it is clearly visible that the aliphatic chains of the triglycerides at the interface tend to orient themselves toward the air phase.

The head groups of triglycerides can form clusters and even merge into extended layers. Three different grades of structuring can be observed for the three investigated temperatures. After 200 ns, the structuring is strongest in the systems with the highest temperature (see Figures 4, 6, and 8). Nevertheless, it is evident in potential energy plots that the systems are not yet in equilibrium after 200 ns simulation time, which is further analyzed and discussed in Sections 3.2 and 4. This means that the most pronounced structuring, which occurs in the system at the highest temperature, arises due to the higher kinetic energy in the system, and the resulting faster dynamics lead to the more rapid discovery of energetically favorable local minima of the potential energy surface, which are more likely to be associated with ordered structures. Therefore, higher temperatures lead to a stronger structuring after 200 ns simulation time.

Nevertheless, this allows for a further conclusion. The structuring of fat at the fat-air interface is quite strong since it is even present at the highest investigated temperature (Figure 4). Therefore, it can be concluded that the structuring effect is not a nucleation effect resulting in liquid to solid transition, as it would be likely below the melting point of POP at 310 K,<sup>[43]</sup> but seems to be a property of the liquid phase. At higher temperatures, it is generally less likely to have ordered molecular structures, due to a higher kinetic energy that keeps the molecules in motion.

The same orientation of aliphatic chains toward the air phase can be observed in the Berger FF simulations, which is shown in Figures 5 and 6. The structuring effects are more pronounced compared to the GAFF simulations after 200 ns. The same effect as with GAFF can be observed when assessing the temperature dependence.

A next level of coarseness is introduced by employing the Martini FF for investigations of the same systems. By mere inspection of the final simulation snapshots, depicted in Figure 7, the orientation at the

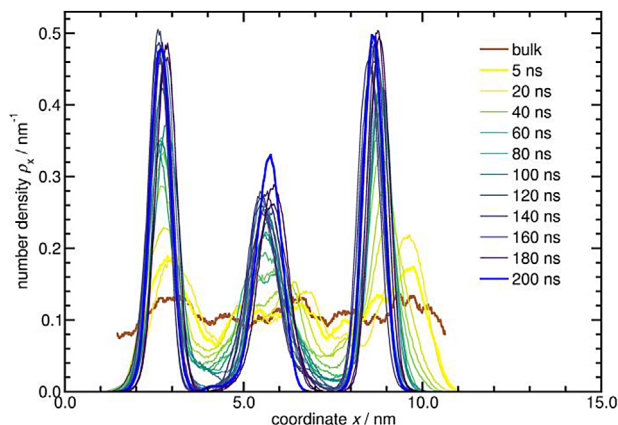


**FIGURE 9** Temporal evolution of the normalized average number densities of glycerol backbones along the  $x$ -axis in 20 ns intervals for the Berger FF at 333 K. The initial bulk simulation (brown), before introducing the air interface, is compared to the extended system with fat-air interface. The yellow line plot with the results of the low peak from the first 5 ns of the production run, and the blue bold line plot with the results of the high peak from the last 5 ns of the production run. The number density plots for the intermediate time intervals are shown with a reduced line width.

interface cannot be seen as clearly as in the simulations with the other two FFs. Nevertheless, in the presented number density plots of the different atoms and beads along the axis perpendicular to the interfaces, the same type of orientation is predicted by the Martini FF, as shown in Figure 8. The structuring is much weaker as in the Berger FF and GAFF simulations (compare Figures 4, 6, and 8).

A significant difference compared to GAFF and Berger FF simulations is that no dominant temperature dependence exists in the simulations with Martini FF. Although it cannot be clearly stated that this difference is only attributable to the not-yet-reached equilibrium states of the GAFF and Berger simulations, it seems likely, which is further discussed and explained in the following sections.

All presented mass density plots show the highest maxima for the two outer glycerol backbone peaks compared to the middle ones. Although it is known that glycerol backbone clustering is also present in pure triglyceride bulk, this shows that the structuring is driven by the interfaces with air and is not pronounced in pure fat bulk systems. This is evidenced by marginal structuring development occurring in bulk during the final 200 ns equilibration step. Pronounced structuring sets in when the fat-air interface is introduced into the system, and structuring is promoted during the production run, as illustrated in Figure 9.

### 3.2 | Equilibrium state analysis

According to Equation (2), the average peak height of the three highest maxima of the number density plots for the glycerol backbones is calculated and plotted over simulation time to reveal the equilibrium state of the structuring effect. When equilibrium is reached, the average peak

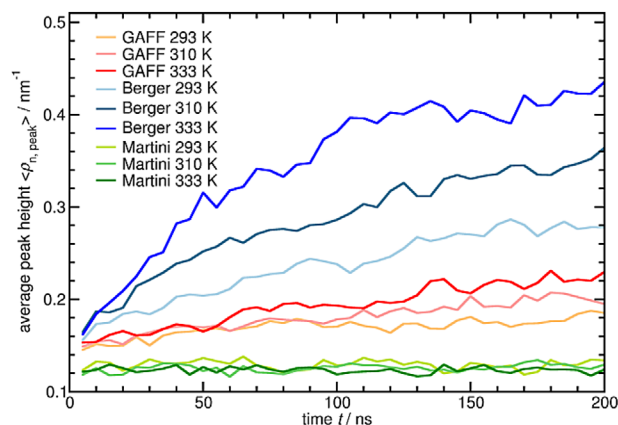


**FIGURE 10** Evolution of the average height of the three highest glycerol number density distribution peaks for all simulated systems.

height should reach a constant value over time with only small thermal fluctuations. To gain a better understanding of the average peak height plots (which are subsequently presented and explained), an example of the time evolution of the number density plots of glycerol backbones is given in Figure 9 using the example of the Berger FF simulation at 333 K. The development of the height of the three highest maxima is a clear descriptor for the presented density distributions and, thus, for the molecular structuring of the system.

Figure 9 illustrates that the structuring effect at the air interface develops during the production run. The pure bulk simulation without a fat-air interface yields marginal fluctuations. Starting from the bold line (yellow) with low and broad peaks (the number density of glycerol backbones during the first 5 ns of the production run), the number density peaks increase and narrow over time, resulting in three distinct maxima. The number density of the last 5 ns time interval (between 195 ns and 200 ns of the production run) is again given as a bold line (blue), resembling the plot of Figure 6 for the glycerol backbone (with a slight shift in height due to smoothing) of the Berger FF simulation at 333 K. The narrower and higher peaks over simulation time mean that the glycerol backbones become increasingly less evenly distributed along the  $x$ -axis and have increasingly more defined positions along the  $x$ -axis. The two outside peaks are higher during all simulation phases, showing that the air interface drives the present structuring effect.

Figure 10 displays the temporal evolution of the average height of the three highest glycerol number density distribution peaks for all simulated systems. It reveals that all three Martini FF simulations (dotted lines) have constant values during the complete production runs and, thus, are in a structural, thermodynamic equilibrium.

The all-atom GAFF simulations have the lowest dynamics since united-atom and coarse-grained FFs usually exhibit a speed-up due to reduced friction when the number of interaction centers is reduced. The average peak height increases slowly at the start of the GAFF simulations. While the slope tends to become less steep, thermodynamic equilibrium is not reached after 200 ns. Nonetheless, it can be stated that the structuring is stronger pronounced than in the simulations with the Martini FF. The Berger FF simulations show the strongest

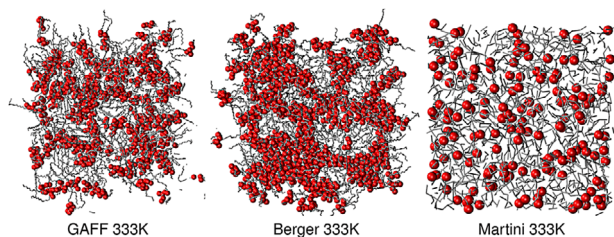


**FIGURE 11** Surface arrangement and cluster formation of POP molecules: glycerol head groups (red) and aliphatic side chains (gray) at the air-POP interface, shown in the  $yz$ -plane at 2.5 nm depth. The interface structures are depicted for GAFF, Berger, and Martini force fields at 333 K.

structuring effects of all models during the whole simulation time. While the slope is high in the beginning, the curves start to level out against the end of the 200 ns simulation time. It can again be stated that the structuring is stronger than in the Martini FF simulations.

Comparing the trajectories of the GAFF and the Berger FF simulations, it also seems probable that the structuring will be more pronounced in the Berger FF than in the GAFF simulations. However, as equilibrium has not been reached, that cannot be stated with certainty.

In the GAFF and Berger FF simulations, it is evident that the structuring is more strongly pronounced in the higher temperature systems. It is not known if this will also hold for the equilibrium structure. In the case of the Martini FF, it is shown that the temperature does not influence structuring since the average peak heights are similar for all three temperatures.

During the development phase of this paper, boxes of different sizes and dimensions resulted in thicker POP films (axis from top to bottom in the presented snapshots of this section) and smaller lateral box sizes (the other two axes of the presented snapshots of this section) were simulated. They always showed the same type of structuring effects at the interfaces. No detailed results are presented here; nevertheless, it is mentioned to strengthen the point that the presented results are not an effect of box dimensions. Of course, finite-size effects can never be completely ruled out since the number of particles cannot be increased to infinity.

### 3.3 | Clustering analysis

In the investigation of the outer layer of POP molecules situated at a depth of 2.5 nm from the air-POP interface, a conspicuous accumulation of glycerol head groups becomes readily apparent (see Figure 11). However, the spatial distribution of these head groups across the  $yz$ -plane is not uniform, which contrasts with POP crystal structures that display extended regions exclusively composed of head groups. Instead, these glycerol head groups tend to self-organize into interconnected clusters, where specific regions showcase notably heightened concentrations. Consequently, a consistent pattern emerges, characterized by regions displaying heightened site-chain accumulations within this layer. This visual observation aligns with the findings pre-

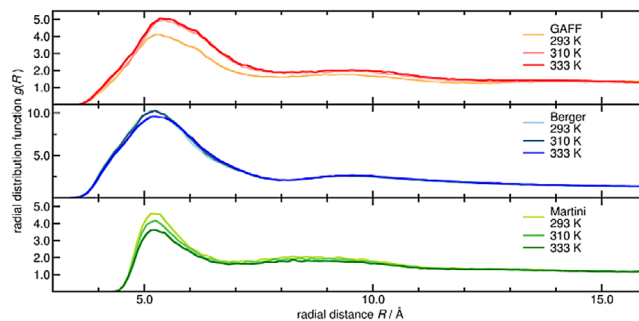


**FIGURE 12** Radial distribution function  $g(R)$  of the central carbon atom of the glycerol group (GAFF, Berger FF) or the glycerol bead (Martini FF). Comparison of  $g(R)$  for simulations using different FFs at temperatures 293 K, 310 K, and 333 K.

sented in the number density plots, wherein only a relatively minor reduction in the density of aliphatic side chains is noticeable at the sites where the accumulation of glycerol backbones is pronounced.

In the following, the formation of clusters is analyzed in terms of the accumulation of head groups of lipids. Therefore, the radial distribution functions  $g(R)$  are determined for the central carbon atom in the glycerol head group or glycerol bead for all morphologies (Figure 12). The radial distribution function  $g(R)$  for the Berger model at 333 K yields a first steep peak at  $R \approx 5.3$  Å and a second broader local maximum at  $R \approx 9.5$  Å, followed by an extended continuum for long radial distances  $R$ . The maxima of  $g(R)$  are slightly shifted to higher values of  $R$  for GAFF, while Martini FF provides maxima at lower values of  $R$ .

The radial distribution function suggests that fat molecules are not randomly distributed within the simulation box but that several head groups form small clusters. This effect is most pronounced in the Berger model, where the height of the radial distribution functions is roughly doubled compared to Martini FF and GAFF.

The coordination numbers  $n_c$  are determined as an average for all fat molecules within the simulation box to indicate cluster formation. Therefore, a nearest neighbor search is carried out for each head group, and the number of neighbors is counted, which are found within a cut-off radius  $R_{\text{cut}}$ , given by the first minimum of the radial distribution function  $g(R)$ . Taking the average for all lipids yields  $n_c$ . The temporal evolution of the average coordination number  $n_c$  shows a clear force field dependence of the cluster formation as well as temperature dependencies (Figure 13). In the case of the Martini FF,  $n_c$  basically oscillates around constant values. As a slight trend, the Martini FF yields a reduction of  $n_c$  with increasing temperature. The observed decrease in coordination number with increasing temperature is consistent with the expected trend for liquid hydrocarbon chains.<sup>[44]</sup> The course of  $n_c$  is therefore another sign that simulations with the Martini FF have quickly reached equilibrium in cluster formation as found in liquids.

In contrast to the Martini FF, GAFF, and Berger FF yield rising trends in  $n_c$  as a function of time superimposed by minor oscillations. The simulations at 333 K show a transition from a rising trend to oscillations around plateau levels at about  $t = 150$  ns for both GAFF and Berger FF. At 293 K and 310 K, the coordination number does not yet settle to a

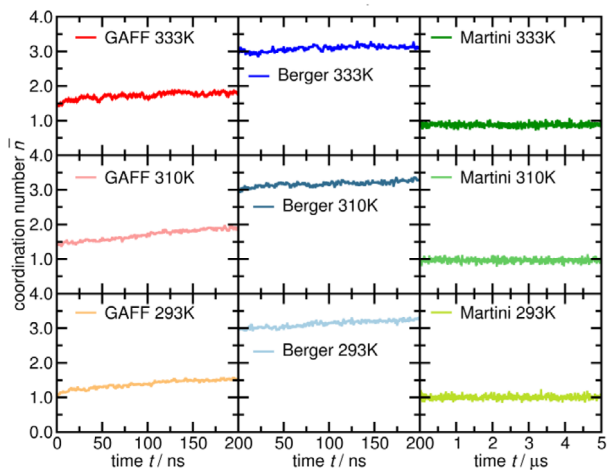


**FIGURE 13** Average coordination number  $n_c$  of the glycerol head groups as a function of simulation time  $t$  for (GAFF, Berger FF, Martini FF) at 293 K, 310 K, and 333 K.

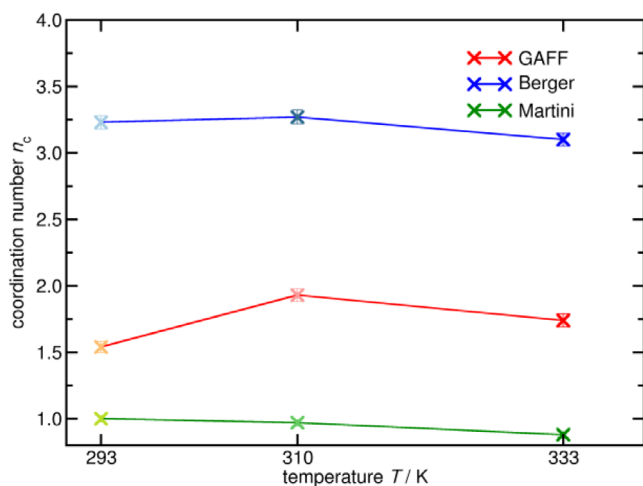


**FIGURE 14** Comparison of average coordination numbers  $n_c$  for simulations using different force fields (GAFF, Berger FF, Martini FF) and temperatures  $T$ .

constant level, indicating that cluster formation is not yet complete at the lower temperatures after the 200 ns production run.

The evolution of the average coordination number  $n_c$  as a function of time indicates the enhanced clustering of glycerol head groups during the simulations. This is consistent with the finding that a higher degree of structuring is achieved with increasing temperature, as indicated in the number density plots (Section 3.1).

Averaging of  $n_c$  is performed over 200 MD frames to quantify the impact of the FF on clustering (Figure 14). The Berger FF yields high coordination numbers  $n_c = 3.20 \pm 0.05$  compared to  $n_c = 1.74 \pm 0.47$  for GAFF and the smallest number for the Martini model  $n_c = 0.95 \pm 0.02$ . Hence, the Berger FF shows the most significant clustering, followed by the GAFF and low clustering for the Martini FF. The reduced  $n_c$  values at 293 K can be ascribed to deviations from the equilibrium conditions for Berger FF and GAFF. Without these deviations, it would

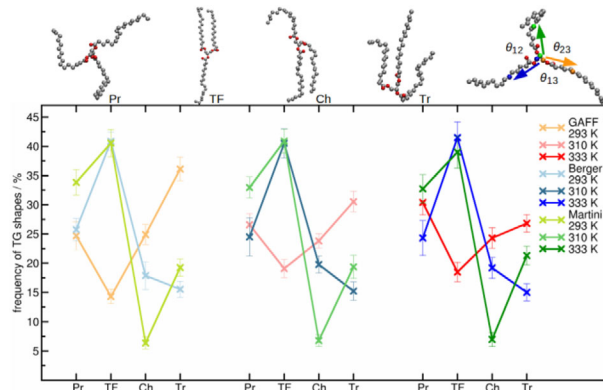


**FIGURE 15** Illustration of structural variations of POP molecules represented by the propeller (Pr), tuning-fork (TF), chair (Ch), and trident (Tr) conformations. The inset provides a schematic depiction of the three vectors describing acyl chain orientations and the three angles used for shape classification. The figure showcases the distribution frequencies of different POP molecule shapes within air-POP interface structures at temperatures for simulations with the GAFF, Berger FF, and Martini FF.

be assumed that the coordination number decreases with temperature according to lower structuring in liquids with higher temperature.<sup>[44]</sup> However, the influence of the temperature on the average coordination number is of minor importance compared to the force field choice. In total, coordination numbers  $n_c$  indicate an inhomogeneous cluster formation of the glycerol head groups during the simulations.

### 3.4 | Intramolecular arrangements of POP

Following the methodology of Tascini et al.,<sup>[2]</sup> a categorization approach is employed to elucidate the primary intramolecular arrangements of POP molecules as they align at the air-POP interface. This categorization system defines four distinct conformational shapes based on the inherent angular relationships within the TG chains (see the graphical definition of  $\theta_{12}$ ,  $\theta_{23}$ , and  $\theta_{13}$  in the inset of Figure 15). The orientation of these chains is determined by the vectors connecting the carbon atoms of the glycerol group with either the sixth atom along each chain (in the cases of the GAFF and Berger FF) or the glycerol bead and the third bead along the chain (as in the Martini FF).

Four distinct classes can be discerned to characterize the conformations of POP molecules: the *propeller* configuration (Pr), characterized by angles evenly distributed, with an average of 120 degrees (also termed the Y-shape); the *tuning-fork* (TF) and *chair* (Ch) conformations, in which two chains align cohesively in the same direction while the third chain opposes this direction—either alternately or with two adjacent chains lying in parallel; and lastly, the *trident* conformation is observed when all three chains uniformly point in a single direction.

The frequency distributions of TG shapes at the interfaces of air-POP are illustrated in Figure 15. For instance, at 333 K in the layered interface structure, the Berger FF demonstrates a predominant occurrence of 41.5% *tuning-fork* shapes, 24.3% *propeller* shapes, 19.2% *chair*



shapes, and 15.0% *trident* shapes. Among these, the *tuning-fork* conformation is most prevalent in both the Berger FF and Martini FF simulations, closely followed by the propeller conformation.

Comparatively, in the Martini FF simulations, there is an increased occurrence of *propeller* and *trident* conformations as opposed to the Berger FF simulations. On the other hand, the GAFF simulations exhibit a reduced prevalence of tuning-fork structures and a more even distribution of shapes, with *trident* conformations taking precedence. Hence, all observed morphologies encompass a mixture of various POP molecule shapes from all four categories, contributing to the establishment of layered structures at the air-POP interface. Compared to the influence of the choice of force field, temperature variations have only a relatively small influence on the distribution of the shapes.

## 4 | DISCUSSION

The presented results show that the structuring at the investigated interface is the same for all considered FFs at all temperatures, which concerns a predominant orientation of the methyl-end groups of the aliphatic chains into the air at the interface and clustering of head groups. However, the extent of structuring differs widely, especially the coarse-grained force field yield distinctions compared to the all-atom and united-atom force fields. Thus, simulation results must be considered with caution.

The results further reveal that the equilibrium is reached after different simulation times, indicating different dynamic behavior at the selected temperatures for different FFs. Only the all-atom simulations can be directly related to physical time scale. United-atom and coarse-grained FFs represent multiple atomic interactions with single beads, leading to a smoothing of the potential energy surface with lower frictional forces, resulting in higher dynamics and higher diffusion coefficients. For this reason, time scales in coarse-grained simulations do not have a one-to-one correspondence with all-atom simulations, and one approximately obtains an acceleration factor of the dynamics of about four.<sup>[45]</sup> This effectively enables extended simulation times with united-atom models and achieves the most prolonged simulation durations for the coarse-grained models. This indicates why equilibrium is reached in the coarse-grained simulations while it is not reached in the all-atom and united-atom simulations.

No clear conclusion can be drawn whether the GAFF or the Berger FF predicts a stronger structuring effect. It is evident that the Berger FF reaches a nearly complete layering of aliphatic chains and glycerol backbones parallel to the interface in the 333 K simulation and can subsequently also reach that in the lower temperature calculations (which should be even more prone to structuring, as they have a lower temperature and thus lower kinetic energy). Whether GAFF might reach the same degree of structuring cannot be said with certainty based on the presented data. Nevertheless, according to the trajectories of the GAFF and Berger FF simulations in Figure 10, it seems unlikely that they will reach the same constant equilibrium value of average peak height.

With the Berger FF and GAFF, the simulations with the highest temperature of 333 K showed the strongest structuring effects (see Figures 4, 6, and 8).

The application of the Berger force field produces simulated mass densities of  $938.1 \pm 0.5 \text{ kg m}^{-3}$  at 293 K,  $928.5 \pm 0.6 \text{ kg m}^{-3}$  at 310 K, and about  $913.6 \pm 0.7 \text{ kg m}^{-3}$  at 333 K. These densities exhibit a reduction when compared to the crystalline phase densities of POP. Notably, the crystalline phase manifests densities of approximately  $974 \pm 1 \text{ kg m}^{-3}$  for the  $\alpha$ -polymorph,  $984 \text{ kg m}^{-3}$  for the  $\gamma$ -polymorph,  $992 \text{ kg m}^{-3}$  for the  $\beta'$ -structure,  $1017 \text{ kg m}^{-3}$  for  $\beta_1$ -structure, and around  $1006 \text{ kg m}^{-3}$  for  $\beta_2$ -structure.<sup>[46]</sup>

Conversely, the densities reported for the liquid state of POP span from 890 to 904  $\text{kg m}^{-3}$ .<sup>[46]</sup> Consequently, the simulated densities employing the Berger FF occupy an intermediary position between the values characterizing pristine crystalline packing arrangements and the fluidic phase of molten POP. These outcomes correspond harmoniously with the structural characteristics elucidated through simulations, which reveal a tendency toward increased local order compared to the liquid phase, even if they do not reach the same degree of crystalline perfection.

## 5 | CONCLUSIONS

A detailed description of the molecular structuring of the triglyceride POP at the fat-air interface is presented in this study by performing molecular dynamics simulations with three different FFs at three different temperatures. They are appropriate for modeling the air-POP interface present in many food systems.

It is demonstrated that POP follows a specific orientation at the air interface. The aliphatic chains are oriented toward the hydrophobic air phase, while the more polar glycerol backbones attract to each other and are positioned in between the aliphatic chains forming small clusters. This has also been reported for triglycerides in nonfood systems in literature.<sup>[1,2]</sup> In this study, it has been shown that this effect is present in simulations with three independently derived molecular dynamics FFs with different degrees of modeling detail.

While the overall type of structuring was the same for all investigated FFs, the extent of structuring differed strongly; the weakest structuring was observed for the Martini FF, which reached equilibrium after 200 ns of the production run. After a simulation time of 200 ns, the Berger FF showed the strongest structuring effects, followed by GAFF. For the latter two force fields, equilibrium was not reached; therefore, no further statements can be made about the extent of their structuring in equilibrium states, except that it is stronger than for the Martini FF. It was shown that the chosen molecular FF significantly impacted the quantitatively obtained data. An estimation of the equilibrium state of the self-assembled structure was presented by tracking the height of the peaks of the number density function along the box axis perpendicular to the interface between the triglycerides and air. Clustering analysis for the glycerol head groups showed in detail the temporal evolution of clustering and provided essentially the same trends for the different

force fields found for structuring by visual inspection and number densities.

Simulations like those presented in this study have been used in the literature to provide insights into the molecular structuring of triglyceride systems. Our investigations show that these results should be treated with great caution.

## AUTHOR CONTRIBUTIONS

Moritz Kindlein: writing—original draft; investigation; visualization; validation; software; data curation; methodology; conceptualization; writing—review & editing. Ekaterina Elts: validation; methodology; conceptualization; writing—review & editing; project administration; supervision. Peter Horlacher: project administration; supervision; resources; funding acquisition; writing—review & editing. Heiko Briesen: funding acquisition; project administration; resources; supervision; formal analysis; writing—review & editing. Tobias Koch: software; writing—original draft; investigation; validation; visualization; writing—review & editing; methodology; data curation; supervision; conceptualization.

## ACKNOWLEDGMENTS

BASF Personal Care and Nutrition GmbH have supported this research.

Open access funding enabled and organized by Projekt DEAL.

## CONFLICT OF INTEREST STATEMENT

The authors have declared no conflict of interest.

## DATA AVAILABILITY STATEMENT

The data that support the findings of this study are available from the corresponding author upon reasonable request.

## ORCID

Tobias Koch  <https://orcid.org/0000-0002-0235-4692>

## REFERENCES

- Wizert, A., Iskander, D. R., & Cwiklik, L. (2014). Organization of lipids in the tear film: A molecular-level view. *PLoS One*, *9*, e92461.
- Tascini, A. S., Noro, M. G., Chen, R., Seddon, J. M., & Bresme, F. (2018). Understanding the interactions between sebum triglycerides and water: A molecular dynamics simulation study. *Physical Chemistry Chemical Physics*, *20*, 1848–1860.
- Eisner, M. D., Jeelani, S. A. K., Bernhard, L., & Windhab, E. J. (2007). Stability of foams containing proteins, fat particles and nonionic surfactants. *Chemical Engineering Science*, *62*, 1974–1987.
- Goff, H. D. (1997). Colloidal aspects of ice cream—A review. *International Dairy Journal*, *7*, 363–373.
- Leser, M. E., & Michel, M. (1999). Aerated milk protein emulsions—New microstructural aspects. *Current Opinion in Colloid & Interface Science*, *4*, 239–244.
- van Aken, G. A. (2001). Aeration of emulsions by whipping. *Colloids and Surfaces A: Physicochemical and Engineering Aspects*, *190*, 333–354.
- Brooker, B. E. (1993). The stabilisation of air in foods containing fat—A review. *Food Structure*, *12*, 12.
- Patino, J. M. R., Delgado, M. D. N., & Fernández, J. L. (1995). Stability and mechanical strength of aqueous foams containing food proteins. *Colloids and Surfaces A: Physicochemical and Engineering Aspects*, *99*, 65–78.
- Hanazawa, T., Sakurai, Y., Matsumiya, K., Mutoh, T. A., & Matsumura, Y. (2018). Effects of solid fat content in fat particles on their adsorption at the air–water interface. *Food Hydrocolloids*, *83*, 317–325.
- Hemming, F. W., & Hawthorne, J. N. (1996). *Lipid analysis* (176 p.). BIOS Scientific Publ.
- Sikorski, Z. E., & Kołakowska, A. (2011). *Chemical, biological, and functional aspects of food lipids* (2nd ed., 497 p.). CRC Press.
- Saunders, M. G., & Voth, G. A. (2013). Coarse-graining methods for computational biology. *Annual Review of Biophysics*, *42*, 73–93.
- Pink, D. A., & Razul, M. S. G. (2014). Computer simulation techniques for food science and engineering: Simulating atomic scale and coarse-grained models. *Food Structure*, *1*, 71–90.
- Marrink, S. J., de Vries, A. H., & Mark, A. E. (2004). Coarse grained model for semiquantitative lipid simulations. *The Journal of Physical Chemistry B*, *108*, 750–760.
- Marrink, S. J., Risselada, H. J., Yefimov, S., Tieleman, D. P., & de Vries, A. H. (2007). The MARTINI force field: Coarse grained model for biomolecular simulations. *The Journal of Physical Chemistry B*, *111*, 7812–7824.
- Berger, O., Edholm, O., & Jahnig, F. (1997). Molecular dynamics simulations of a fluid bilayer of dipalmitoylphosphatidylcholine at full hydration, constant pressure, and constant temperature. *Biophysical Journal*, *72*, 2002–2013.
- Chen, G., Huang, K., Miao, M., Feng, B., & Campanella, O. H. (2019). Molecular dynamics simulation for mechanism elucidation of food processing and safety: State of the art. *Comprehensive Reviews in Food Science and Food Safety*, *18*, 243–263.
- Nian, B., Xu, Y. J., & Liu, Y. (2021). Molecular dynamics simulation for mechanism revelation of the safety and nutrition of lipids and derivatives in food: State of the art. *Food Research International*, *145*, 110399.
- Kindlein, M., Greiner, M., Elts, E., & Briesen, H. (2015). Interactions between phospholipid head groups and a sucrose crystal surface at the cocoa butter interface. *Journal of Physics D: Applied Physics*, *48*, 384002.
- Greiner, M., Sonnleitner, B., Mailänder, M., & Briesen, H. (2014). Modeling complex and multi-component food systems in molecular dynamics simulations on the example of chocolate conching. *Food & Function*, *5*, 235–242.
- Green, N. L., Euston, S. R., & Rousseau, D. (2019). Interfacial ordering of tristearin induced by glycerol monooleate and PGPR: A coarse-grained molecular dynamics study. *Colloids and Surfaces B: Biointerfaces*, *179*, 107–113.
- Brasiello, A., Crescitelli, S., & Milano, G. (2011). Development of a coarse-grained model for simulations of tridecanoin liquid–solid phase transitions. *Physical Chemistry Chemical Physics*, *13*, 16618–16628.
- Brasiello, A., Crescitelli, S., & Milano, G. (2012). A multiscale approach to triglycerides simulations: From atomistic to coarse-grained models and back. *Faraday Discuss*, *158*, 479–492.
- Pizzirusso, A., Brasiello, A., Nicola, A. d., Marangoni, A. G., & Milano, G. (2015). Coarse-grained modelling of triglyceride crystallisation: A molecular insight into tripalmitin tristearin binary mixtures by molecular dynamics simulations. *Journal of Physics D: Applied Physics*, *48*, 494004.
- Pizzirusso, A., Peyronel, F., Co, E. D., Marangoni, A. G., & Milano, G. (2018). Molecular insights into the eutectic tripalmitin/tristearin binary system. *Journal of the American Chemical Society*, *140*, 12405–12414.
- van der Spoel, D., Lindahl, E., Hess, B., Groenhof, G., Mark, A. E., & Berendsen, H. J. C. (2005). GROMACS: Fast, flexible, and free. *Journal of Computational Chemistry*, *26*, 1701–1718.

27. Hockney, R. W., Goel, S. P., & Eastwood, J. W. (1974). Quiet high-resolution computer models of a plasma. *Journal of Computational Physics*, *14*, 148–158.
28. Wang, J. M., Wolf, R. M., Caldwell, J. W., Kollman, P. A., & Case, D. A. (2004). Development and testing of a general amber force field. *Journal of Computational Physics*, *25*, 1157–1174.
29. de Silva, A. W. S., & Vranken, W. F. (2012). ACPYPE—AnteChamber PYthon Parser interface. *BMC Research Notes*, *5*, 1–8.
30. Wang, J., Wang, W., Kollman, P. A., & Case, D. A. (2006). Automatic atom type and bond type perception in molecular mechanical calculations. *Journal of Molecular Graphics and Modelling*, *25*, 247–260.
31. Wang, J., Wang, W., Kollman, P. A., & Case, D. A. (2001). Antechamber: An accessory software package for molecular mechanical calculations. *Journal of Chemical Information and Computer Sciences*, *222*, 1–41.
32. Jakalian, A., Bush, B. L., Jack, D. B., & Bayly, C. I. (2000). Fast, efficient generation of high-quality atomic charges. AM1-BCC model: I. Method. *Journal of Computational Chemistry*, *21*, 132–146.
33. Walker, R. C., Crowley, M. F., & Case, D. A. (2008). The implementation of a fast and accurate QM/MM potential method in Amber. *Journal of Computational Chemistry*, *29*, 1019–1031.
34. Stewart, J. J. P. (1990). *MOPAC 6 manual* (6th ed., pp. 1–207). F. J. Seiler Research Laboratory United States Air Force Academy.
35. Dewar, M. J. S., Zoebisch, E. G., Eamonn, F., & Stewart, J. J. P. (1985). Development and use of quantum mechanical molecular models. 76. AM1: A new general purpose quantum mechanical molecular model. *Journal of the American Chemical Society*, *107*, 3902–3909.
36. Bush, B. L., Bayly, C. I., & Halgren, T. A. (1999). Consensus bond-charge increments fitted to electrostatic potential or field of many compounds: Application to MMFF94 training set. *Journal of Computational Chemistry*, *20*, 1495–1516.
37. Darden, T. T., York, D., & Pedersen, L. (1993). Particle mesh Ewald: An  $N \cdot \log(N)$  method for Ewald sums in large systems. *The Journal of Chemical Physics*, *98*, 10089–10092.
38. Tieleman, P. Berger Lipid Force Field Download of Topologies. Accessed Juli 23, 2019. <http://wcm.ucalgary.ca/tieleman/downloads>
39. Marrink, S. J. (2013). Martini force field download of topologies. Accessed November 9, 2017. <http://md.chem.rug.nl/index.php/force-field-parameters>
40. Bussi, G., Donadio, D., & Parrinello, M. (2007). Canonical sampling through velocity rescaling. *The Journal of Chemical Physics*, *126*, 14101.
41. Berendsen, H. J. C., Postma, J. P. M., van Gunsteren, W. F., DiNola, A., & Haak, J. R. (1984). Molecular dynamics with coupling to an external bath. *The Journal of Chemical Physics*, *81*, 3684–3690.
42. Parrinello, M., & Rahman, A. (1981). Polymorphic transitions in single crystals: A new molecular dynamics method. *Journal of Applied Physics*, *52*, 7182–7190.
43. Ghazani, S. M., & Marangoni, A. G. (1921). Molecular origins of polymorphism in cocoa butter. *Annual Review of Food Science and Technology*, *12*, 567–590.
44. Eduljee, G. H. (1982). A note on the temperature dependence of the coordination number. *Fluid Phase Equilibria*, *9*, 41–47.
45. Marrink, S. J., & Tieleman, D. P. (2013). Perspective on the Martini model. *Chemical Society Reviews*, *42*, 6801–6822.
46. Arishima, T., Sagi, N., Mori, H., & Sato, K. (1995). Density measurement of the polymorphic forms of POP, POS and SOS. *Journal of Oleo Science*, *44*, 431–437.

**How to cite this article:** Kindlein, M., Elts, E., Horlacher, P., Briesen, H., & Koch, T. (2023). Structuring of 2-oleodipalmitin at the air interface from all-atom, united-atom, and coarse-grained molecular dynamics simulations. *European Journal of Lipid Science & Technology*, *125*, e2300110. <https://doi.org/10.1002/ejlt.202300110>